Insights into the Responding Modes of Highly Potent Gadolinium-Based Magnetic Resonance Imaging Probes Sensitive to Zinc Ions

Gaoji Wang, Harlei Martin, Susana Amézqueta, Clara Ràfols, Goran Angelovski, Celia Bonnet

Insights into the Responding Modes of Highly Potent Gadolinium-based MRI Probes Sensitive to Zinc Ions

Gaoji Wang,[1,2] Harlei Martin,[3] Susana Amézqueta,[4,5] Clara Ràfols,[4,5] Célia S. Bonnet[3,*] and Goran Angelovski,[1,6,*]

[1] MR Neuroimaging Agents, Max Planck Institute for Biological Cybernetics, Tuebingen, Germany

[2] School of Chemistry and Chemical Engineering, Jiangsu University, Zhenjiang 212013, PR China

[3] Centre de Biophysique Moléculaire, UPR 4301 CNRS, Rue Charles Sadron, Université d'Orléans, Orléans, 45071, France.

[4] Departament d'Enginyeria Química i Química Analítica, Facultat de Química, Universitat de Barcelona (UB), c/ Martí i Franquès, 1, 08028 Barcelona, Spain.

[5] Institut de Biomedicina (IBUB), Universitat de Barcelona (UB), 08028 Barcelona, Spain.

[6] Laboratory of Molecular and Cellular Neuroimaging, International Center for Primate Brain Research (ICPBR), Center for Excellence in Brain Science and Intelligence Technology (CEBSIT), Chinese Academy of Sciences (CAS), 20031 Shanghai, PR China.

ABSTRACT: Zinc ions (Zn^{2+}) play an important biological role in many diseases, hence an imaging method for monitoring the Zn^{2+} distribution in tissues could provide important clinical insights. Recently, we reported a potent Zn-sensitive probe based on the Gd-DO3A (DO3A – 1,4,7,10-tetraazacyclododecane-1,4,7-tricarboxylic acid), modified tyrosine and DPA (di-(2-picolyl)amine) chelator for this metal cation, which generates outstanding magnetic resonance imaging (MRI) response. Here we further explored the origin of this unprecedented response and expanded the choice of the potential MRI probes by preparing the free acid version of the initial MRI sensor. We report a detailed investigation of the ^{1}H nuclear magnetic relaxation dispersion (NMRD), ^{17}O NMR and isothermal titration calorimetry properties of these two MRI probes upon interacting with Zn^{2+}. The performed experiments confirm the selective interaction of the MRI probes and the target metal cation, which causes substantial changes in the coordination sphere of the paramagnetic center. It also evidenced some aggregation which enhances the relaxivity response. Interestingly, conversion of the methyl ester to the free carboxylic acid of tyrosine moiety changes the nature of the aggregates and leads to a smaller relaxivity response. The probes interact with human serum albumin (HSA) in the absence of Zn^{2+}, which leads to a possible modification of the coordination sphere of Gd^{3+} or a substantial change in the exchange rate of second sphere water molecules. In the presence of Zn^{2+}, the interaction with HSA is very weak, demonstrating the importance of the Zn^{2+} coordination sphere in the behavior of these systems.

INTRODUCTION

Zinc ions (Zn^{2+}) are essential for the occurrence of many biological processes in the human body.[1,2] Both their excess and deficiency may result in organs' dysfunction;[3] hence, the detection of Zn^{2+} can be helpful for the diagnosis of related diseases. Sensing Zn^{2+} by means of magnetic resonance imaging (MRI) has attracted significant attention lately, due to the affirmative features of this powerful molecular imaging technique.[4] Consequently, a wide range of the so-called "smart" or responsive MRI contrast agents have been designed to provide response to Zn^{2+}.[5-14]

Among these, paramagnetic complexes based on Gd^{3+} are the most exploited candidates for the development of Zn^{2+}-sensitive MRI contrast agents.[15-18] In most cases, Gd^{3+} is chelated and stabilized by macrocyclic ligands such as 1,4,7,10-tetraazacyclododecane-1,4,7-tricarboxylic acid (DO3A).[4, 19] In these complexes, the Gd^{3+} coordination sphere is completed by water molecule(s) that exchange with the bulk, thereby changing the T_1 relaxation time and consequently enhancing the image contrast in the T_1-weighted imaging. The ability of the MRI probe at a defined concentration (1 mM) to influence the T_1 relaxation time is known under the term relaxivity and is proportional to q, the number of bound water molecules. Alteration of

the *q* number causes dramatic relaxivity changes of the MRI probe, resulting in a response of the so-called *q*-modulated agents, which can indicate changes in the local concentration of the targeted metal ions. Following this mechanism, Meade and coworkers designed Zn^{2+}-activated MRI agents consisting of a GdDO3A moiety and a Zn-binding domain.[5, 20] Once the agents interacted with Zn^{2+}, the acetate groups "flipped" away from Gd^{3+}, resulting in an increase in the hydration number and an enhancement of relaxivity by up to 200%.

Additionally, the water proton relaxivity of Zn^{2+}-specific MRI probes can be largely enhanced in the presence of human serum albumin (HSA), particularly at medium magnetic fields (20-80 MHz).[21] Indeed, the formation of these adducts results in a decrease in the rotational correlation time of the system (τ_R), and therefore a relaxivity enhancement. Sherry and coworkers initially developed a diDPA-based agent (DPA – di-(2-picolyl)amine).[22] Its complex with Zn^{2+} did not result in a large relaxivity change; however, the entire chelate with Zn^{2+} built a ternary complex with HSA that led to a 3-fold relaxivity enhancement. Following this example, a series of DPA-based agents were prepared. Their relaxometric properties were investigated upon addition of Zn^{2+} and HSA at low magnetic fields (0.5 T), where the change in relaxivity is the highest.[8, 22] When investigating these at the high field (9.4 T), their relaxivity response was also sufficient to allow exciting MR imaging studies of Zn^{2+} release *in vivo* upon glucose-stimulated insulin secretion in mouse pancreas[8, 9, 23] and prostate showing different zinc release between healthy and cancerous tissues.[24] Additionally, an interesting tool to increase the response of such τ_R-based systems at high fields is the fast-field cycling (FFC) MRI.[25-27] This approach was recently demonstrated on a probe that did not show any Zn^{2+} response at 3 T using MRI, while using the FFC-MRI at the same field, its response was restored.[28]

Inspired by aforementioned approaches, we used tyrosine as a tether to connect a GdDO3A moiety and a Zn^{2+}-binding domain DPA. The structural transformation of the phenoxy group of the tyrosine into the phenoxyacetic acid paved the way to achieving large relaxivity enhancement ("turn-on" mechanism) upon Zn^{2+} addition. Namely, the recently reported complex **GdL¹**, which bears a modified tyrosine as the methyl ester, underwent a significant relaxivity boost in the presence of Zn^{2+} at 7 T, showing to be highly potent for Zn^{2+} imaging.[29] A further possible and straightforward change in the structure of **GdL¹** is conversion of the amino methyl ester to the amino acid, which may result in a change in features of the paramagnetic complex and its interaction with Zn^{2+}. Hence, we hydrolyzed the amino methyl ester to obtain the complex **GdL²** (Chart 1). Following its preparation, we performed a detailed investigation of the relaxometric properties of two analogous gadolinium complexes **GdL¹·²**. We recorded their ^1H NMR dispersion (NMRD) and ^{17}O NMR spectra at different temperatures, in presence of Zn^{2+} and human serum albumin (HSA), and in their absence. We also studied their interaction with Zn^{2+} by means of the isothermal titration calorimetry (ITC) experiments. Comparison of the obtained results could provide valuable information for the future design of even more potent MRI sensors for studying Zn^{2+}.

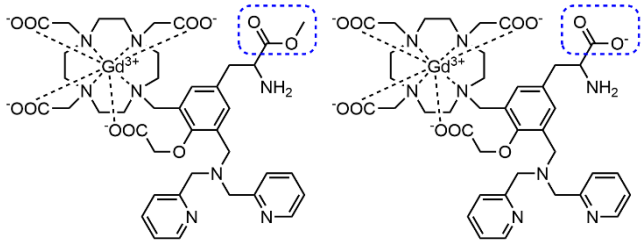

Chart 1. Complexes **GdL¹** and **GdL²** discussed in the present work. Blue dashed rectangles indicate the difference between these molecules, i.e. **GdL¹** is a methyl ester (left) and **GdL²** is an acid (right).

RESULTS AND DISCUSSION

Synthesis of the ligand and lanthanide complexes

Ligand **L²** was obtained by the base hydrolysis of the methyl ester of the compound **L¹**, in analogy with the previously published procedure, except that NaOH was used instead of LiOH.[30] Subsequently, Gd^{3+} or Tb^{3+} complexes with **L²** to enable studying their relaxometric or luminescence properties, respectively, were obtained by direct reaction of the ligand with the appropriate lanthanide metal nitrate in water.

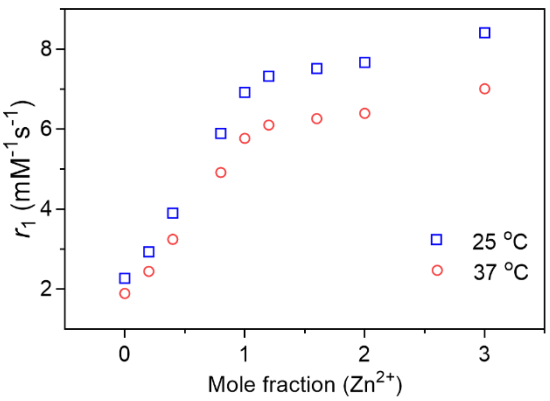

Figure 1. Relaxometric titration of **GdL²** (1 mM) with Zn^{2+} at 7 T at 25 °C and 37 °C in PBS (pH 7.4).

Relaxometric titrations at 7T

To compare the relaxometric response of newly prepared **GdL²** with the previously studied **GdL¹**, we performed its

titration with Zn^{2+} at 7T magnetic field strength.[29] The experiments were performed in PBS and HEPES at 25 °C and 37 °C by adding small aliquots of Zn^{2+} and calculating r_1 value after each addition of the metal ion (Figure 1 and Figure S1 in Supporting Information). As in the case of its ester analogue (**GdL¹**), **GdL²** displays strong r_1 response that reaches 270 % enhancement relative to the initial value in PBS at both temperatures and slightly lower enhancement in HEPES depending on the temperature (267% and 150% at 25 °C and 37 °C, respectively). These results showed that Zn^{2+} strongly affects the T_1 values of **GdL²**, albeit concurrently exhibiting differences in the amplitude of response compared to **GdL¹** (in HEPES: 400% and 300% at 25 °C and 37 °C, respectively; in PBS: 300% and 280% at 25 °C and 37 °C, respectively).[29] It was also shown that this interaction is reversible, as upon addition of one equivalent of a strong metal ion chelator such as ethylenediaminetetraacetic acid (EDTA), the relaxivity of **GdL²**–Zn went back to the initial value of **GdL²** (Figure S2 in Supporting Information). Being intrigued by these differences and reasons for slightly different behavior, we performed detailed investigations that included NMRD and ^{17}O NMR experiments (see below). Prior to that, we estimated the hydration number, *q*, using the luminescent coordination analogue of **GdL²** (**TbL²**), and assessed the interaction of both **GdL¹** and **GdL²** with Zn^{2+} using the ITC.

Table 1. Luminescence lifetimes of the **TbL¹·²** (1 mM) in H_2O and D_2O with and without Zn^{2+}, and the calculated *q* values. The luminescence lifetime and *q* values for **TbL¹** were determined previously and serve for better comparison with the analogue values for **TbL²**.[29]

	TbL only			TbL + Zn^{2+} (2 equiv.)			
	τ_{H_2O} (ms)	τ_{D_2O} (ms)	q	τ_{H_2O} (ms)	τ_{D_2O} (ms)	q	Δq
TbL¹	1.91	1.96	0.0	1.30	2.37	1.4	1.4
TbL²	1.90	2.10	0.0	1.31	2.26	1.3	1.3

Determination of the hydration number, *q*

The number of water molecules directly coordinated to Gd^{3+}, *q*, is important since it greatly influences the longitudinal relaxivity of the complex; consequently, the changes in *q* strongly affect the r_1 values. To determine *q*, the luminescence lifetimes of **TbL²** in H_2O and D_2O were investigated at 25 °C and the hydration number values were abstracted from the obtained lifetimes (Table 1). In the absence of Zn^{2+}, **TbL²** is non-hydrated, which is consistent with the very low initial r_1 value of **GdL²**. Upon Zn^{2+} addition, the *q* number of **TbL²** is 1.3, which is comparable to the value observed for **TbL¹** (0 and 1.4 in the absence and presence of Zn^{2+}, respectively). Based on the results for r_1 and *q*, the extra carboxylate function in **GdL²** compared to **GdL¹** does not play an important role in modifying the Gd^{3+} coordination sphere upon Zn^{2+} complexation, which could be explained by the following possibilities: (1) it remains coordinated to Gd^{3+}, whether Zn^{2+} is present or not; (2) it is never coordinated; (3) the arm switches between Gd^{3+} coordination and Zn^{2+} coordination, which is accompanied with a change in the overall coordination number of Gd^{3+}. All together, these results suggest that the two complexes likely undergo the same mechanism upon Zn^{2+} coordination with a substantial change in the coordination sphere of the Gd-DO3A unit.

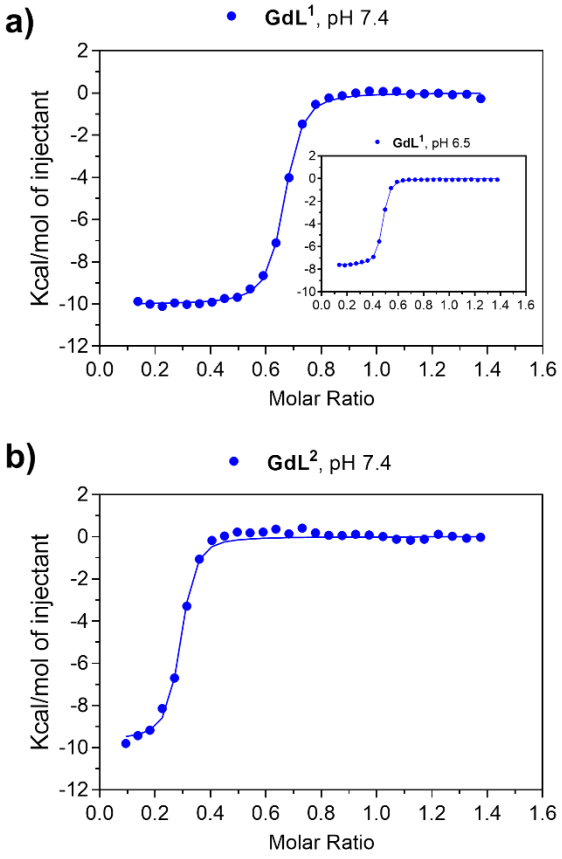

Figure 2. Binding isotherms obtained in the ITC experiment of a) **GdL¹** and b) **GdL²** with Zn^{2+} in HEPES (pH 7.4, I=150 mM). The inset in a) represents the ITC experiment of **GdL¹** performed at pH 6.5, where the red dots indicate values obtained from the blank.

Isothermal titration calorimetry experiments

In order to characterize the interaction of **GdL¹** and **GdL²** with Zn^{2+}, ITC experiments were performed (Figure 2). The binding of **GdL¹** to Zn^{2+} was evaluated in HEPES at pH 7.4 and 6.5 and the ion strength (I) = 150 mM. The pH 6.5 was chosen for comparison purposes, as Zn^{2+} might precipitate at pH 7.4 (visually imperceptible at the working conditions).[31] At pH 6.5, a stoichiometry n of *ca.* 0.5 was found. This matches the observation reported previously,[29] which could be associated to the formation of **GdL¹**-Zn-**GdL¹** complex (Figure 2a, inset). The binding constant logarithm

is log K = 7.2 (±0.1), with n=0.40 (±0.06). However, despite the consistent preparation of **GdL¹** and Zn^{2+} solutions (same buffer, solutions equilibration before ITC experiments, etc.), the binding stoichiometry was not reproducible in all repetitions. In a group of experiments, we observed that the binding constant logarithm was of the same order of magnitude (log K = 6.8 (±0.2)) but with a n=0.13 (±0.04). We hypothesize that **GdL¹** underwent an aggregation process even at these low concentrations (0.3 mM), which is difficult to control. Notwithstanding, even in the presence of aggregates (n~0.1), the Zn^{2+} binding occurs. Regarding the enthalpy (ΔH) of the process, values were similar for all the replicates (-8.5 (±0.6) kcal).

Similar behavior was observed at pH 7.4, where stoichiometries varied in the range 0.1-0.7 (Figure 2a). Those interactions that occurred at n 0.3-0.7 presented a binding constant logarithm of log K = 7.2 (±0.2), and when aggregation took place (n~0.1), a log K value of 6.8 (±0.1) was observed. The interaction event was slightly more exothermic (ΔH = -9.6 (±0.6) kcal) than the process at pH 6.5.

The binding of **GdL²**-Zn^{2+} by means of the ITC was studied at the biorelevant pH 7.4 (Figure 2b). In this case, observed stoichiometries varied in the range 0.1-0.3, indicating that **GdL²** tends to aggregate with higher ability than **GdL¹** at these concentrations. Aggregates were also able to interact with Zn^{2+} in an exothermic way (ΔH = -10 (±4) kcal), and the interaction binding logarithm (log K = 7.0 (±0.2)) was similar to that of **GdL¹**.

Overall, the ITC studies indicated that both complexes tend to aggregate in the presence of Zn^{2+}, possibly through different aggregation processes. Namely, the presence of an extra carboxylate group in **GdL²** gives rise to the larger portion of the formed aggregates. Still, both complexes bind Zn^{2+} with *ca.* 100 nM affinity, which is in the range of other binding constants observed with DPA units.[13]

NMRD and ^{17}O NMR experiments

NMRD profiles are commonly used to characterize the parameters governing proton relaxivity of contrast agents. Thus, the ^1H NMRD profiles of aqueous solutions of **GdL¹** and **GdL²** were recorded at 25 and 37 °C and pH 7.4 in the field range of 0.04 - 600 MHz (Figure 3). The relaxivity of both complexes decreases with increasing temperature, which is characteristic of low molecular weight, fast tumbling systems. The low longitudinal relaxivities of 2.62 $mM^{-1}s^{-1}$ and 2.58 $mM^{-1}s^{-1}$ at 20 MHz and 25 °C for **GdL¹** and **GdL²**, respectively, point to the absence of any water molecules in the first coordination sphere of the Gd^{3+} center. Interestingly, in the presence of Zn^{2+}, the relaxivity profiles show a hump at intermediate fields (20-80 MHz), characteristic of slow rotating species. Dramatic relaxivity enhancements upon Zn^{2+} coordination of *ca.* 400 % and 250 % were observed for **GdL¹** and **GdL²**, respectively, at 40 MHz and 25°C or 37°C. This highlights the efficacy of these complexes as responsive contrast agents for Zn^{2+} detection.

In order to rationalize these observations and understand the differences observed between **GdL¹** and **GdL²**, we performed a complete analysis of the systems to obtain a reliable picture of the important microscopic parameters determining relaxivity.

Analysis of the relaxation properties of the complexes in the absence of Zn^{2+}. In the absence of Zn^{2+}, the number of water molecules directly coordinated to Gd^{3+} is zero (Table 1), which means that only the water molecules diffusing around Gd^{3+} will contribute to the relaxivity (outer-sphere mechanism). However, the data could not be fitted by using a purely outer-sphere ABHF (Ayant-Belorisky-Hwang-Fried) model. This can be explained by the presence of many hydrophilic functions, which can give rise to a second-sphere contribution to relaxivity. This second sphere contribution concerns water molecules that are retained in the vicinity of Gd^{3+} by hydrogen bonding for example.

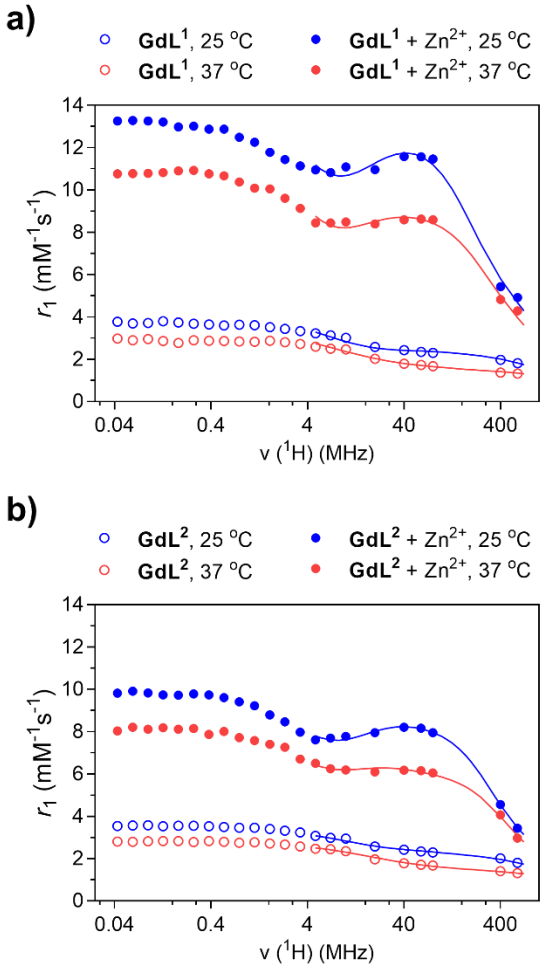

Figure 3. ^1H NMRD profiles of a) [**GdL¹**] and b) [**GdL²**] (both 0.9 mM) at 25°C and 37°C in absence and presence of Zn^{2+}, (0.9 and 0.83 mM for **GdL¹** and **GdL²**, respectively), in HEPES (0.1 M, pH 7.4). The lines represent the fit obtained with the SBM theory (integrating the Lipari-Szabo approach for **GdL²**+Zn^{2+}).

Therefore, we fitted the NMRD data using the Solomon–Bloembergen–Morgan (SBM) theory. The fit was restricted to frequencies above 4 MHz, as at low magnetic fields the theory fails in describing the electronic parameters. Several parameters were fixed to the common values, such as: the number of water molecules directly coordinated to Gd^{3+} was set to q=0, the relative diffusion coefficient was set to D_{GdH}^{298} = 2.6 x 10^{-9} m^2 s^{-1} and the activation energy of the modulation of the zero-field splitting was set to E_v = 1 kJ mol^{-1}. To describe the second sphere contribution, the Gd-H distance was fixed to 4.5 Å, and the exchange rate of the second sphere water was assumed to be very fast, more specifically k_{ex} = 2 x 10^9 s^{-1}.[32, 33] In reality, the exchange of the second sphere water is too fast to have any impact on the fitting. The rotational correlation time (τ_r), its activation energy (E_r), the activation energy of the relative diffusion coefficient (E_{DGdH}) and the electronic parameters, i.e. the mean square of the zero-field splitting (Δ^2) and the correlation time for the modulation of the zero-field splitting (τ_v^{298}) were fitted, but these electronic parameters should not be over-interpreted (Table S1, Supporting Information). The best fit was obtained, for both complexes, by assuming one second sphere water molecule (q^{SS} = 1) at 4.5 Å from Gd^{3+}, which is a very small contribution, albeit necessary to reproduce the experimental data. The two complexes gave very similar parameters, and we can infer that the extra carboxylate is either coordinated or does not play an important role in the overall relaxivity of the complex in the absence of Zn^{2+}; in any case, it does not have an important second sphere relaxivity contribution.

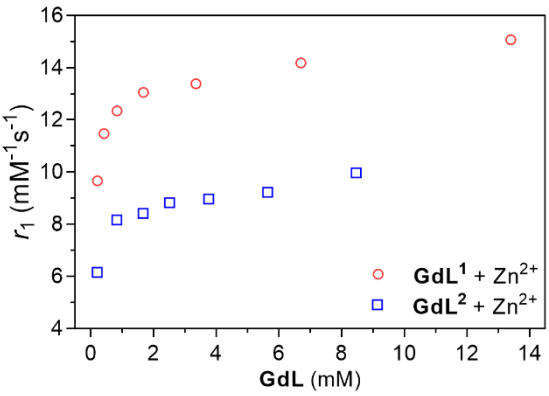

Figure 4. Relaxivity of **GdL¹** + Zn^{2+} (red circles) and **GdL²**+Zn^{2+} (blue squares) at 60 MHz (25 °C, pH = 7.4) as a function of concentration.

Analysis of the relaxation properties of the complexes in the presence of Zn^{2+}. The ^{1}H NMRD profiles of **GdL¹⁻²** in the presence of Zn^{2+} show a hump at intermediate fields (20-80 MHz), characteristic of slow rotating species (see above). As the Gd-L complexes remain small molecular systems, this points to aggregation processes as also evidenced by ITC experiments (see above). We therefore measured the relaxivity as a function of concentration to investigate aggregation processes. For this, we screened the r_1 values of **GdL¹** + Zn^{2+} and **GdL²** + Zn^{2+} solutions at the concentrations ranging from 0.2 mM to >10 mM. The data showed a variation of relaxivity with concentration, even at concentrations as low as 0.2 mM (Figure 4). It should be noted that in the absence of Zn^{2+}, **GdL¹** shows some small aggregation process, while **GdL²** does not (Figure S3 in Supporting information), which already underlines the different behavior of the two complexes due to the presence of the extra carboxylate. These results clearly indicated concentration-depended processes, likely the aggregate formation, to influence the relaxivity of the studied complexes that can be noticed at the studied magnetic field strength (60 MHz).

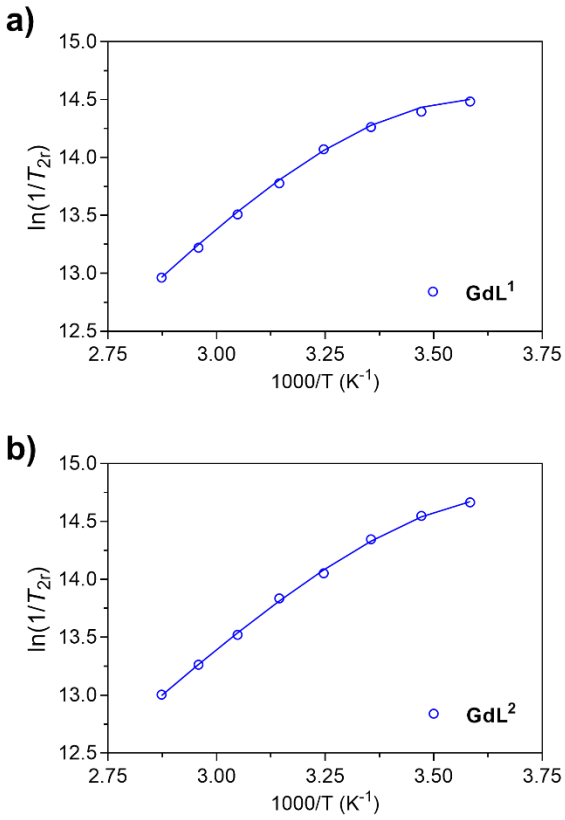

Figure 5. Temperature dependence of reduced ^{17}O transverse relaxation rates of a) **GdL¹**+Zn^{2+} and b) **GdL²**+Zn^{2+} at 9.4 T.

To gain further information on the microscopic parameters governing the relaxivity of **GdL¹⁻²** in the presence of Zn^{2+}, variable temperature ^{17}O NMR experiments were also recorded (Figure 5). For both species the T_1 values were too close to those of the reference to yield reliable data, and the peaks were too broad to obtain reliable chemical shifts. Hence, only ^{17}O T_2 were analyzed, which give access to the water exchange rate, k_{ex}. The reduced ^{17}O transverse relaxation rates decrease with increasing temperature, indicating that the complexes are in the fast exchange region at all temperatures and that the observed T_2 relaxation rates are dominated by the relaxation rate of the bound water.

In the fast exchange region, $1/T_{2r}$ is determined by the transverse relaxation rate of the coordinated water oxygen, $1/T_{2m}$, which is in turn influenced by the water exchange rate, k_{ex}, the longitudinal electronic relaxation rate, $1/T_{1e}$, and the scalar coupling constant, $A/\hbar$. Due to the different concentrations used for ^{17}O NMR (approx. 13-14 mM) and NMRD samples (approx. 1 mM), and the aggregation process evidenced above, the ^{17}O NMR and the NMRD profiles were fitted separately.

Table 2. Main parameters obtained from the fitting of the NMRD and ^{17}O NMR data. Underlined parameters have been fixed. SS stands for second-sphere.

	GdL^1	GdL^1 + Zn^{2+}	GdL^2	GdL^2 + Zn^{2+}
q	0	1	0	1
q^{SS}	1	-	1	-
k_{ex}^{298} (10^6 s^{-1})	-	22 (1)	-	27 (2)
$\Delta H^{\neq}$ (kJ.mol^{-1})	-	30 (1)	-	26 (1)
$k_{ex}^{298\,SS}$ (10^6 s^{-1})	2000	-	2000	-
$\Delta H^{\neq SS}$ (kJ.mol^{-1})	30	-	30	-
r_{GdH} (Å)	4.5	3.1	4.5	3.1
E_g (kJ/mol)	-	23 (3)	-	21 (2)
τ_g^{298} (ps)	-	840 (40)	-	500 (20)
E_l [(/mol)	-	10 (4)	-	10 (5)
τ_l^{298} (ps)]	-	250 (20)	-	50 (3)
S^2	-	0.3 (1)	-	0.38 (2)

Fitting of the ^{17}O NMR data with the Solomon-Bloembergen and Morgan (SBM) theory yielded k_{ex}^{298} values of 22 × 10^6 s^{-1} for **GdL^1** and 27 × 10^6 s^{-1} for **GdL^2** (see Table 2 and Table S2 in the Supporting Information for full set of parameters). We checked that reasonable variation of the electronic parameters did not affect significantly this exchange rate. These values are in the same order of magnitude for the two complexes, meaning that the extra carboxylate function in **GdL^2** vs **GdL^1** does not play an important role in accelerating the water exchange rate. These rates are fast for monohydrated complexes; as a comparison for GdDOTA, k_{ex} = 4.1 × 10^6 s^{-1}.[34] This could be explained by the presence of the tyrosine, which induces steric compression around the water binding site, known to increase k_{ex}.[34] The presence of extra hydrophilic functions able to form hydrogen bonds with the inner sphere water molecules, and/or the presence of Zn^{2+} in close proximity could also accelerate this exchange.

Due to the presence of small aggregates at 1 mM, rotational dynamics could be only described by applying the Lipari-Szabo approach during the data fitting. Using this methodology, the local and global motions, characterized by the local and global rotational correlation times, τ_l^{298} and τ_g^{298}, respectively, were separated and a model independent order parameter, S^2, was used. It reflects the degree of spatial restriction of the local motion with respect to the global motion. Its value ranges from 0 to 1, with S^2 = 0 if the internal motions are isotropic, and S^2 = 1 if the internal motions are completely restricted.

The fit yielded global correlation times for **GdL^1** + Zn^{2+} and **GdL^2** + Zn^{2+} of 840 and 500 ps, respectively. This reflects the presence of aggregates of smaller size in the case of **GdL^2**. The local correlation times were also very different for the two complexes. While τ_l^{298} is close to that of GdDTPA or GdDOTA for **GdL^2** (50 ps),[35] it is 5 times longer for **GdL^1** (250 ps). This is consistent with the concentration-dependent relaxivity experiments of **GdL^1** in absence of Zn^{2+} (see above and Figure S2 in Supporting Information), also meaning that the motion of the Gd^{3+} complex is more restricted in **GdL^1** than in **GdL^2**. The S^2 values were similar for the two complexes, showing similar rigidities for the two systems, and were in the same order of magnitude as the micellar systems[36] or other aggregated complexes.[37, 38]

The results obtained from the fitting the experimental data according to the SBM theory confirmed the existence of the aggregates in these samples. Moreover, the lower relaxivity observed for **GdL^2** vs **GdL^1** in the presence of Zn^{2+} can likely be explained by the existence of smaller and more flexible aggregates, despite the similar chemical structure of the complexes.

Relaxivity of the complexes in the presence of HSA

The **GdL^1** and **GdL^2** complexes were titrated against HSA (0 to 1 mM), the most abundant protein in the blood. For both systems the relaxivity increases with increasing HSA concentration in the absence of Zn^{2+} ions (Figure 6a-b). This is indicative of an interaction between the complex and HSA as was previously observed for other systems containing DPA in the absence[28] or in the presence[22] of Zn^{2+}.

The titration was performed in excess of HSA compared to the complexes. In these conditions, it is possible to fit the data obtained to determine the site of highest affinity. The data were fitted to obtain the K_D values (Eq. 1) for the site of highest affinity in HSA, and a model with one binding site could be used (Eq. 2), where r_1^f and r_1^b represent the relaxivity of the complex in the free and bound state, respectively, c_1 and c_{HSA} are the complex and HSA concentrations, respectively, and $K_A = 1/K_D$ is the affinity constant.

GdL + HSA = GdL-HSA (Eq. 1)

$$R_1^{p,obs} = 10^3 \times \left(\left(r_1^f \cdot c_1\right) + \frac{1}{2}\left(r_1^b - r_1^f\right) \times \left(c_{HSA} + c_1 + K_A^{-1} - \sqrt{(c_{HSA} + c_1 + K_A^{-1})^2 - 4 \cdot c_{HSA} \cdot c_1}\right)\right) \quad \text{(Eq. 2)}$$

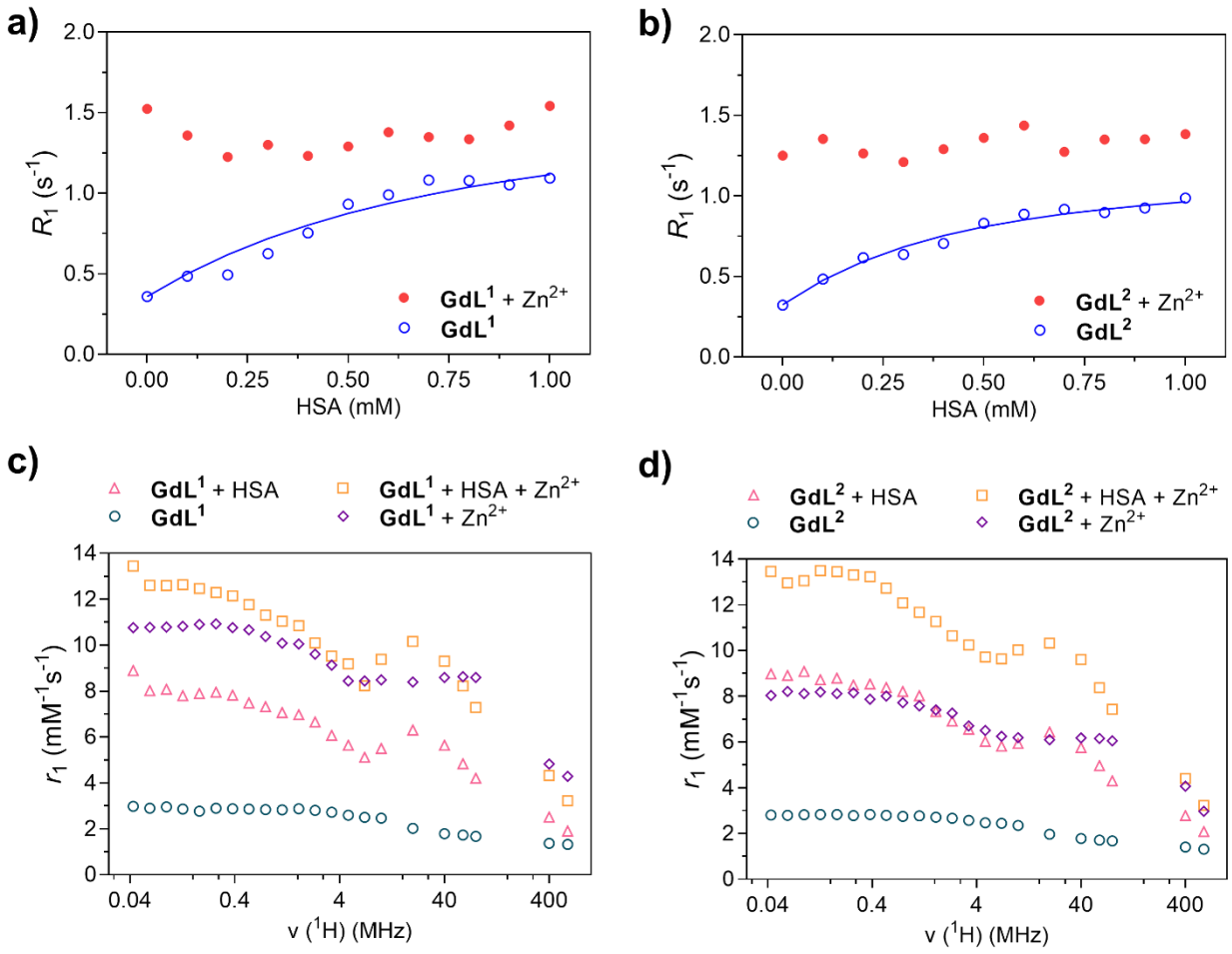

Figure 6: Relaxometric experiments of **GdL¹** and **GdL²** with HSA in presence and absence of Zn^{2+}. a-b) Relaxation rates as a function of concentration of HSA at 37°C and at 60 MHz in HEPES (0.1 M, pH 7.4) with concentration of **GdL¹⁻²** as follows: a) [**GdL¹**] = 0.2 mM and [**GdL¹+Zn**] = 0.175 mM; b) [**GdL²**] = 0.185 mM and [**GdL²+Zn**] = 0.185 mM. c-d) ^{1}H NMRD profiles of **GdL¹⁻²** at 37°C in HEPES (0.1 M, pH 7.4), in the absence/presence of HSA (0.6 mM) and in the absence/ presence of 1 eq. of Zn^{2+}, where: c) [**GdL¹**] = 0.256 mM and [**GdL¹+Zn**] = 0.266 mM, d) [**GdL²**] = 0.229 mM and [**GdL²+Zn**] = 0.228 mM.

The K_D values obtained were 660 μM for **GdL¹**-HSA and 320 μM for **GdL²**-HSA. Both values are in the low mM range, indicating weak interaction with HSA, with twice stronger interaction of **GdL²** compared to that of **GdL¹**. This can probably be explained by the presence of the extra carboxylate function, as these functions are known to interact with cationic residues at the surface of the protein.

The NMRD profiles of the two complexes in the presence of physiological concentrations of HSA (0.6 mM) were recorded at 37 °C (Figure 6c-d). In the conditions used for the experiment, and using the K_D values, we can calculate that 43% of **GdL¹** is interacting with HSA, while 59% of **GdL²** is interacting with HSA. The NMRD profiles are therefore a weighted average of the profiles of GdL and GdL-HSA. In these conditions, it is difficult to obtain reliable data for the GdL-HSA species. Nevertheless, some conclusions can be drawn from these NMRD profiles. Conversely to what was observed in the absence of HSA and in the absence of Zn^{2+}, the characteristic hump of slowly rotating species at intermediate fields (20-80 MHz) is present for both complexes. This shows that in the presence of HSA, there are certainly some water molecules directly bound to Gd^{3+} and/or the second sphere water molecules present in the absence of HSA have a much smaller exchange rate due to the presence of the protein. Consequently, such process displays the visible effect on the rotational correlation time of the system.

In the presence of Zn^{2+}, relaxivities of **GdL¹** and **GdL²** do not significantly change with HSA addition at 60 MHz (Figures 6a-b). However, the NMRD profiles of **GdL¹-Zn** and **GdL²-Zn** ternary complexes in the absence and in the presence of HSA are not the same at all fields (Figure 6c-d). It should also be noted that at the working concentration, and at particular fields, the relaxivity of **GdL²-Zn** and **GdL²-HSA** is the similar, which should always be a point-of-care for *in vivo* studies for any systems. Interestingly, in the presence of Zn^{2+} and HSA, the NMRD profiles of **GdL¹**

and **GdL²** becomes similar. This is indicative of: (1) different aggregation states of both complexes alone and in the presence of HSA and (2) a weak interaction of the GdL-Zn complexes with HSA. In any case, this interaction is much smaller than what was reported for other Zn^{2+}-responsive systems containing the DPA unit.[8, 23] In the latter cases, the coordination sphere of Zn^{2+} in the complexes was not complete, and the formation of ternary GdL-Zn-HSA complexes was observed. The case of **GdL¹** and **GdL²** is different, as the complexes possess at least one extra carboxylate coordinating function, plus other possible coordinating groups (one amine and either a carboxylate or an ester function). This means that the Zn^{2+} coordination sphere is certainly saturated by the complex, preventing the formation of ternary species with HSA.

CONCLUSIONS

We have developed two Gd^{3+} complexes showing unprecedented relaxivity increase upon Zn^{2+} binding. These relaxivity increases are mainly explained by the switch of the carboxylate arm from the tyrosine from Gd^{3+} to Zn^{2+}, leading to a change in the hydration number of Gd^{3+} upon Zn^{2+} coordination. Extensive relaxometry and ITC experiments evidenced the presence of aggregates, which enhances the relaxivity response in the presence of Zn^{2+}, especially at intermediate magnetic fields (20 -80 MHz). Interestingly, the conversion of the ester arm in the previously reported GdDO3A contrast agent (**GdL¹**) into a carboxylate function (**GdL²**), is slightly detrimental to the Zn^{2+} response. This can be rationalized in terms of the size of the aggregates, which are smaller for **GdL²**, and their nature, as they are more rigid in the case of **GdL¹**. Finally, both complexes showed to interact with HSA in the absence of Zn^{2+} in the low mM range. This interaction either leads to a change in the coordination sphere of Gd^{3+} (the complexes become hydrated), or/and accelerates significantly the exchange rate of second-sphere water molecules. In the presence of Zn^{2+}, the interaction of the complexes with HSA was very small.

In summary, this study shows that the *q*-switch (change in the Gd^{3+} coordination sphere) is still the major cause for the observed and strong relaxivity changes, albeit the presence of aggregates enhances the response at intermediate fields. The nature and size of the aggregates is substantially altered by small molecular changes. These aggregation phenomena, which have a strong impact on the Zn^{2+} response *in vitro*, remain very difficult to predict in biological media, especially due to the modification of these aggregates in the presence of HSA. Finally, we show that, additionally to influencing the Gd^{3+} coordination sphere, the Zn^{2+} coordination is also important to define the relaxivity response in the presence of HSA. Therefore, the behavior of these complexes *in vivo* will be dependent on many parameters, namely the local concentration of the complex, the interaction with HSA, temperature, and obviously the presence of zinc. The insights obtained in this study will be very valuable for the future design and preparation of viable and biocompatible smart probes, and their use in the functional MRI studies.

EXPERIMENTAL SECTION

General remarks. $ZnCl_2$ (catalogue number: 1.08816), HEPES (catalogue number: H3375), KOH (catalogue number: 1.09918), HCl (catalogue number: 1.09970) and albumin from human serum (catalogue numbers A3782) were purchased from Sigma-Aldrich. ^{1}H and ^{13}C NMR spectra were obtained at 25 ºC using a Bruker Avance III 300 MHz spectrometer. The concentration of Gd^{3+} and Tb^{3+} in analyzed solutions were determined using the bulk magnetic susceptibility shift (BMS) method.[39] Low resolution mass spectra were obtained on an ion trap SL 1100 system Agilent with an electrospray ionization source.

Ligand L². Compound **L¹** (0.074 g, 0.09 mmol) and NaOH (0.011 g, 0.27 mmol) were stirred in methanol (3 mL) for 12 h at 25 °C. After removing solids by the filtration, methanol solution was evaporated. The crude mixture was dissolved in water, the pH was adjusted to 7 and the mixture was purified by HPLC. Yield of **L²** was 0.057 g (79%). **^{1}H NMR** (D_2O, 300 MHz): 2.61–3.69 (br, 24H, C*H*$_2$); 3.75–4.12 (br, 12H, C*H*$_2$); 7.17, 7.65 (s, 2H, phenolic); 7.32 (t, *J*= 6.0 Hz, 2H, NCHC*H*), 7.47 (d, *J*= 7.4 Hz, 2H, NCC*H*), 7.78 (t, *J*= 7.4 Hz, 2H, CCHC*H*), 8.42 (d, *J*= 3.7 Hz, 2H, NC*H*CH); **^{13}C NMR** (D_2O, 75 MHz): 34.4 (1C, ArCH_2CH); 48.3–55.5 (15C); 70.7 (1C, ArOCH_2); 125.7, 126.4, 127.1, 129.3, 132.3 (11C); 141.1, 147.2 (6C, pyridyl); 151.8 (2C, NCHCH); 155.8 (1C, NCHCO); 169.1 (2C, NCCH); 171.0 (5C, *C*O). LC-MS: (*m*/*z*) $[M-H]^-$ Calcd. for $C_{39}H_{52}N_8O_{11}^-$: 808.5. Found: 808.5.

Preparation of the complexes and solutions. Both complexes were prepared by reaction of a solution of $Ln(NO_3)_3{\cdot}6H_2O$ (0.04 mmol) and **L²** (0.023 g, 0.04 mmol) in water (10 mL), following the same procedure as previously described.[29] All the complexes are purified by HPLC and subsequently freeze-dried.

Complex GdL². LRMS: (*m*/*z*) $[M-H]^-$ Calcd. for $C_{39}H_{49}GdN_8O_{11}^-$: 962.3. Found: 962.3.

Complex TbL². LRMS: (*m*/*z*) $[M-H]^-$ Calcd. for $C_{39}H_{49}TbN_8O_{11}^-$: 963.3. Found: 963.3.

Luminescence lifetimes. The luminescence lifetimes of the complex **TbL²** (1 mM) were measured in D_2O and H_2O with and without Zn^{2+} (2 equiv.) at 25 °C (50 mM HEPES, pH 7.4). The Tb^{3+} ion was directly excited at λ_{ex} = 283 nm and the emission spectra were recorded by calculating the lifetime values at λ_{max} = 546 nm. Both excitation and emission slits were 10 nm. The resulting *q* value, which denotes the hydration number of coordinated water molecules, was then calculated using the equation (Eq. 3).[40]

$$q(Tb) = 5 \times (1/\tau_{H_2O} - 1/\tau_{D_2O} - 0.06) \qquad \text{(Eq. 3)}$$

ITC Measurements. A Microcal VP-ITC (MicroCal, LLC, Northampton, MA, USA) titrator was used. Working

solutions were degassed by means of a Thermovac (MicroCal, LLC) vacuum degasser. A Crison micro-pH 2002 potentiometer (Crison Instruments, Alella, Spain) equipped by a Crison 5014 combination electrode was used for p*H* measurements. To perform the ITC measurements, first a 0.250 mM HEPES buffer solution neutralized with KOH was prepared. An adequate amount of HCl was added to an aliquot of the previous solution to get the chosen pH value (6.50 or 7.40, depending on the experiment), and lastly diluted to a final concentration of 0.150 mM. Working in this way, the ion strength of the buffers is 150 mM (biorelevant ion strength). To prepare the different buffers, water purified by a Milli-Q-plus system with a resistance higher than 18 MΩ·cm was employed.

GdL¹ (0.3 mM), **GdL²** (0.3 mM) and $ZnCl_2$ (0.05 mM) solutions were prepared using HEPES buffer at I=150 mM and pH 6.50 or 7.40, depending on the experiment. Prior to their use, solutions were degassed for 5 min. ITC titrations were performed at 25.0 ± 0.5 ˚C (preliminary studies did not show significant differences of binding parameters with temperatures in the range 25-37ºC). The power reference was 10 μcal s^{-1} and the stirring rate was 290 rpm. The calorimetric cell was filled in with the corresponding GdL solution. Next, 29 independent additions (10 μL) of the $ZnCl_2$ solution were done. The interval between injections was 300 s to warrant the equilibrium in each titration point. Background titrations were performed by adding identical titrant solution over the cell filled just with the buffer. These measurements allow determining the background heat to be subtracted to the main titration due to the $ZnCl_2$ dilution and/or the mixing. Each assay was repeated minimum four times. Experimental data were collected automatically by the ITC device, and analyzed using the integrated Origin 7.0 software to get the interaction stoichiometry, *n*, and the binding parameter associated to the interaction event, ΔH and K_b.

Relaxometric Measurements. ^{1}H NMR longitudinal relaxometric titrations with $ZnCl_2$ were performed at 7 T, pH 7.4 (50 mM HEPES or PBS buffer) and 25 °C or 37 °C, using the inversion recovery (T_1) pulse sequence. A ZnCl2 solution of known concentration was added stepwise to the gadolinium solution (starting concentration 3.0 mM Gd^{3+}), and the values of T_1 were recorded after each addition of the analyte. The r_1 values were calculated from Eq. 4, where $T_{1,obs}$ is the measured T_1, $T_{1,d}$ is the diamagnetic contribution of the solvent, and [Gd] is the actual Gd^{3+} concentration at each point of the titration.

$$\frac{1}{T_{1,obs}} = \frac{1}{T_{1,d}} + r_1 \times [Gd] \qquad \text{(Eq. 4)}$$

^{1}H NMRD profiles were recorded on a Stelar SMARTracer Fast Field Cycling relaxometer (0.04 – 10 MHz) and a Bruker WP80 NMR electromagnet adapted to variable field measurements (20 – 80 MHz) and controlled by a SMARTracer PC-NMR console. The temperature was monitored by a VTC91 temperature control unit and maintained by a gas flow. The temperature was determined by previous calibration with a Pt resistance temperature probe. Relaxivity at 400 MHz and 600 MHz were measured on a Bruker Ascend 400 and an Oxford AS 600 spectrometers, respectively. The solutions were inserted into capillary tubes and placed into a 5mm NMR tube using DMSO-d_6 as an external reference to lock the spectrometer. The GdL solutions were made in HEPES buffer (0.1 M) at pH 7.4 and at the following concentrations for the GdL complexes: **GdL¹** – 0.9 mM, **GdL²** – 0.9 mM, **GdL¹+Zn** – 0.9 mM, **GdL²+Zn** – 0.83 mM, **GdL¹+HSA** – 0.256 mM, **GdL²+HSA** – 0.229 mM, **GdL¹+Zn+HSA** – 0.266 mM, **GdL²+Zn+HSA** – 0.256 mM. The concentrations of Gd^{3+}-containing solutions were confirmed both by ICP and BMS measurements when possible. The least-square fit of the ^{1}H NMRD data was performed by using Visualizeur/Optimiseur[41] running on a MATLAB 8.3.0 (R2014a) platform.

The HSA titrations of **GdL¹** and **GdL²**, as well as the concentration effects, were performed at 60 MHz on a Bruker Minispec MQ-60 relaxometer. For the HSA titrations, the solutions were made up in HEPES buffer (0.1 M, pH 7.4) and the concentrations of the GdL solutions were kept constant: [**GdL¹**] = 0.2 mM, [**GdL¹+Zn**] = 0.175 mM, [**GdL²**] = 0.185 mM, [**GdL²+Zn**] = 0.185 mM, while the HSA concentration was varied from 0 mM to 1 mM.

Temperature-dependent ^{17}O NMR measurements. The transverse and longitudinal ^{17}O NMR relaxation rates ($1/T_2$, $1/T_1$) and the chemical shifts were measured in aqueous solutions of **GdL¹⁻²+Zn** in the temperature range 278-348 K, on a Bruker Avance 400 (9.4 T, 54.5 MHz) spectrometer. The temperature was calculated according to previous calibration with ethylene glycol and methanol.[42] An acidified water solution ($HClO_4$, pH 3.3) was used as external reference. Transverse relaxation times (T_2) were obtained by the Carr-Purcell-Meiboom-Gill spin-echo technique.[43] The technique of the ^{17}O NMR measurements on Gd^{3+} complexes has been described elsewhere.[44] The samples were sealed in glass spheres fitted into 10 mm NMR tubes to avoid susceptibility corrections of the chemical shifts.[45] To improve the sensitivity ^{17}O-enriched water (10 % $H_2{}^{17}O$, CortectNet) was added to reach around 1 % enrichment. The concentrations and pH of solutions were as follows: [**GdL¹+Zn**] = 14.48 mM, pH 5.1 and [**GdL²+Zn**] = 12.75 mM, pH 5.5. The least-square fit of the ^{17}O NMR were performed using Visualiseur/Optimiseur[41] running on a MATLAB 8.3.0 (R2014a) platform.

AUTHOR INFORMATION

Corresponding Authors

*E-mail: celia.bonnet@cnrs.fr (C. B.)
*E-mail: goran.angelovski@icpbr.ac.cn (G. A.)

ACKNOWLEDGMENT

We thank Agnès Pallier for performing some relaxivity measurements. The financial support of China Scholarship Council (PhD fellowship to Gaoji Wang), the Ministerio de Ciencia, Innovación y Universidades from the Spanish

Government (PID2020-115374GB-I00), La Maison de la Chimie, La Ligue Contre le Cancer, the Shanghai Municipal Science and Technology Major Project (Grant No. 2019SHZDZX02) and the National Natural Science Foundation of China (Grant No. 22174154) is gratefully acknowledged.

REFERENCES

1. Vallee, B. L.; Auld, D. S. Zinc Coordination, Function, and Structure of Zinc Enzymes and Other Proteins. *Biochemistry* **1990,** 29 (24), 5647-5659 DOI: 10.1021/bi00476a001.

2. Costello, L. C.; Fenselau, C. C.; Franklin, R. B. Evidence for operation of the direct zinc ligand exchange mechanism for trafficking, transport, and reactivity of zinc in mammalian cells. *J. Inorg. Biochem.* **2011,** 105 (5), 589-599 DOI: 10.1016/j.jinorgbio.2011.02.002.

3. Mills, C. F. In *Zinc in Human Biology*; Mills, C. F., Ed.; Springer London: London, 1989; pp 371-381.

4. Wahsner, J.; Gale, E. M.; Rodríguez-Rodríguez, A.; Caravan, P. Chemistry of MRI Contrast Agents: Current Challenges and New Frontiers. *Chem. Rev.* **2019,** 119 (2), 957-1057 DOI: 10.1021/acs.chemrev.8b00363.

5. Major Jody, L.; Parigi, G.; Luchinat, C.; Meade Thomas, J. The synthesis and in vitro testing of a zinc-activated MRI contrast agent. *Proc. Natl. Acad. Sci. U.S.A.* **2007,** 104 (35), 13881-13886 DOI: 10.1073/pnas.0706247104.

6. Zhang, X.-a.; Lovejoy Katherine, S.; Jasanoff, A.; Lippard Stephen, J. Water-soluble porphyrins as a dual-function molecular imaging platform for MRI and fluorescence zinc sensing. *Proc. Natl. Acad. Sci. U.S.A.* **2007,** 104 (26), 10780-10785 DOI: 10.1073/pnas.0702393104.

7. Stasiuk, G. J.; Minuzzi, F.; Sae-Heng, M.; Rivas, C.; Juretschke, H. P.; Piemonti, L.; Allegrini, P. R.; Laurent, D.; Duckworth, A. R.; Beeby, A.; Rutter, G. A.; Long, N. J. Dual-Modal Magnetic Resonance/Fluorescent Zinc Probes for Pancreatic beta-Cell Mass Imaging. *Chem. Eur. J.* **2015,** 21 (13), 5023-5033 DOI: 10.1002/chem.201406008.

8. Yu, J.; Martins, A. F.; Preihs, C.; Jordan, V. C.; Chirayil, S.; Zhao, P. Y.; Wu, Y. K.; Nasr, K.; Kiefer, G. E.; Sherry, A. D. Amplifying the Sensitivity of Zinc(II) Responsive MRI Contrast Agents by Altering Water Exchange Rates. *J. Am. Chem. Soc.* **2015,** 137 (44), 14173-14179 DOI: 10.1021/jacs.5b09158.

9. Lubag, A. J. M.; De Leon-Rodriguez, L. M.; Burgess, S. C.; Sherry, A. D. Noninvasive MRI of beta-cell function using a Zn^{2+}-responsive contrast agent. *Proc. Natl. Acad. Sci. U.S.A.* **2011,** 108 (45), 18400-18405 DOI: 10.1073/pnas.1109649108.

10. Mishra, A.; Pariani, G.; Oerther, T.; Schwaiger, M.; Westmeyer, G. G. Hyperpolarized Multi-Metal ^{13}C-Sensors for Magnetic Resonance Imaging. *Anal. Chem.* **2016,** 88 (22), 10790-10794 DOI: 10.1021/acs.analchem.6b03546.

11. Tirukoti, N. D.; Avram, L.; Haris, T.; Lerner, B.; Diskin-Posner, Y.; Allouche-Arnon, H.; Bar-Shir, A. Fast Ion-Chelate Dissociation Rate for In Vivo MRI of Labile Zinc with Frequency-Specific Encodability. *J. Am. Chem. Soc.* **2021,** 143 (30), 11751-11758 DOI: 10.1021/jacs.1c05376.

12. Bar-Shir, A.; Yadav, N. N.; Gilad, A. A.; van Zijl, P. C. M.; McMahon, M. T.; Bulte, J. W. M. Single ^{19}F Probe for Simultaneous Detection of Multiple Metal Ions Using miCEST MRI. *J. Am. Chem. Soc.* **2015,** 137 (1), 78-81 DOI: 10.1021/ja511313k.

13. Bonnet, C. S.; Caillé, F.; Pallier, A.; Morfin, J.-F.; Petoud, S.; Suzenet, F.; Tóth, É. Mechanistic Studies of Gd^{3+}-Based MRI Contrast Agents for Zn^{2+} Detection: Towards Rational Design. *Chem. Eur. J.* **2014,** 20 (35), 10959-10969 DOI: 10.1002/chem.201403043.

14. Malikidogo, K. P.; Da Silva, I.; Morfin, J.-F.; Lacerda, S.; Barantin, L.; Sauvage, T.; Sobilo, J.; Lerondel, S.; Tóth, É.; Bonnet, C. S. A cocktail of 165Er(iii) and Gd(iii) complexes for quantitative detection of zinc using SPECT and MRI. *Chem. Commun.* **2018,** 54 (55), 7597-7600 DOI: 10.1039/c8cc03407a.

15. Bonnet, C. S. Zn^{2+} detection by MRI using Ln^{3+}-based complexes: The central role of coordination chemistry. *Coord. Chem. Rev.* **2018,** 369, 91-104 DOI: 10.1016/j.ccr.2018.04.019.

16. Li, H.; Meade, T. J. Molecular Magnetic Resonance Imaging with Gd(III)-Based Contrast Agents: Challenges and Key Advances. *J. Am. Chem. Soc.* **2019,** 141 (43), 17025-17041 DOI: 10.1021/jacs.9b09149.

17. Heffern, M. C.; Matosziuk, L. M.; Meade, T. J. Lanthanide Probes for Bioresponsive Imaging. *Chem. Rev.* **2014,** 114 (8), 4496-4539 DOI: 10.1021/cr400477t.

18. Malikidogo, K. P.; Martin, H.; Bonnet, C. S. From Zn(II) to Cu(II) Detection by MRI Using Metal-Based Probes: Current Progress and Challenges. *Pharmaceuticals* **2020,** 13 (12), DOI: 10.3390/ph13120436.

19. Clough, T. J.; Jiang, L.; Wong, K.-L.; Long, N. J. Ligand design strategies to increase stability of gadolinium-based magnetic resonance imaging contrast agents. *Nat. Commun.* **2019,** 10 (1), 1420 DOI: 10.1038/s41467-019-09342-3.

20. Matosziuk, L. M.; Leibowitz, J. H.; Heffern, M. C.; MacRenaris, K. W.; Ratner, M. A.; Meade, T. J. Structural Optimization of Zn(II)-Activated Magnetic Resonance Imaging Probes. *Inorg. Chem.* **2013,** 52 (21), 12250-12261 DOI: 10.1021/ic400681j.

21. Aime, S.; Barge, A.; Botta, M.; Terreno, E. In *Metal Ions in Biological Systems: The Lanthanides and Their Interrelations with Biosystems*; Sigel, A., Sigel, H., Ed.; Marcel Dekker, Inc.: New York, Basel, 2003; Chapter 16, Vol. 40, pp 643-682.

22. Esqueda, A. C.; Lopez, J. A.; Andreu-De-Riquer, G.; Alvarado-Monzon, J. C.; Ratnakar, J.; Lubag, A. J. M.; Sherry, A. D.; De Leon-Rodriguez, L. M. A New Gadolinium-Based MRI Zinc Sensor. *J. Am. Chem. Soc.* **2009,** 131 (32), 11387-11391 DOI: 10.1021/ja901875v.

23. Martins, A. F.; Jordan, V. C.; Bochner, F.; Chirayil, S.; Paranawithana, N.; Zhang, S. R.; Lo, S. T.; Wen, X. D.; Zhao, P. Y.; Neeman, M.; Sherry, A. D. Imaging Insulin Secretion from Mouse Pancreas by MRI Is Improved by Use of a Zinc-Responsive MRI Sensor with Lower Affinity for Zn^{2+} Ions. *J. Am. Chem. Soc.* **2018,** 140 (50), 17456-17464 DOI: 10.1021/jacs.8b07607.

24. Clavijo Jordan, M. V.; Lo, S.-T.; Chen, S.; Preihs, C.; Chirayil, S.; Zhang, S.; Kapur, P.; Li, W.-H.; De Leon-Rodriguez Luis, M.; Lubag Angelo, J. M.; Rofsky Neil, M.; Sherry, A. D. Zinc-sensitive MRI contrast agent detects differential release of Zn(II) ions from the healthy vs. malignant mouse prostate. *Proc. Natl. Acad. Sci. U.S.A.* **2016,** 113 (37), E5464-E5471 DOI: 10.1073/pnas.1609450113.

25. Lurie, D. J.; Aime, S.; Baroni, S.; Booth, N. A.; Broche, L. M.; Choi, C.-H.; Davies, G. R.; Ismail, S.; Ó hÓgáin, D.; Pine, K. J. Fast field-cycling magnetic resonance imaging. *C.R. Phys.* **2010,** 11 (2), 136-148 DOI: 10.1016/j.crhy.2010.06.012.

26. Bödenler, M.; de Rochefort, L.; Ross, P. J.; Chanet, N.; Guillot, G.; Davies, G. R.; Gösweiner, C.; Scharfetter, H.; Lurie, D. J.; Broche, L. M. Comparison of fast field-cycling magnetic resonance imaging methods and future perspectives. *Mol. Phys.* **2019,** 117 (7-8), 832-848 DOI: 10.1080/00268976.2018.1557349.

27. Hoelscher, U. C.; Lother, S.; Fidler, F.; Blaimer, M.; Jakob, P. Quantification and localization of contrast agents using

delta relaxation enhanced magnetic resonance at 1.5 T. *Magn. Reson. Mater. Phys., Biol. Med.* **2012,** 25 (3), 223-231 DOI: 10.1007/s10334-011-0291-6.

28. Bödenler, M.; Malikidogo, K. P.; Morfin, J.-F.; Aigner, C. S.; Tóth, É.; Bonnet, C. S.; Scharfetter, H. High-Field Detection of Biomarkers with Fast Field-Cycling MRI: The Example of Zinc Sensing. *Chem. Eur. J.* **2019,** 25 (35), 8236-8239 DOI: 10.1002/chem.201901157.

29. Wang, G.; Angelovski, G. Highly Potent MRI Contrast Agent Displaying Outstanding Sensitivity to Zinc Ions. *Angew. Chem. Int. Ed.* **2021,** 60 (11), 5734-5738 DOI: 10.1002/anie.202014431.

30. Wang, G.; Platas-Iglesias, C.; Angelovski, G. Europium(III) Macrocyclic Chelates Appended with Tyrosine-based Chromophores and Di-(2-picolyl)amine-based Receptors: Turn-On Luminescent Chemosensors Selective to Zinc(II) Ions. *ChemPlusChem* **2020,** 85 (5), 806-814 DOI: 10.1002/cplu.201900731.

31. Ringbom, A. *Complexation in analytical chemistry : a guide for the critical selection of analytical methods based on complexation reactions*. R. E. Krieger Pub. Co., 1979: Huntington, N.Y., 1963.

32. Lebdušková, P.; Hermann, P.; Helm, L.; Tóth, É.; Kotek, J.; Binnemans, K.; Rudovský, J.; Lukeš, I.; Merbach, A. E. Gadolinium(iii) complexes of mono- and diethyl esters of monophosphonic acid analogue of DOTA as potential MRI contrast agents: solution structures and relaxometric studies. *Dalton Trans.* **2007,** (4), 493-501 DOI: 10.1039/b612876a.

33. Laine, S.; Morfin, J.-F.; Galibert, M.; Aucagne, V.; Bonnet, C. S.; Tóth, É. Lanthanide DO3A-Complexes Bearing Peptide Substrates: The Effect of Peptidic Side Chains on Metal Coordination and Relaxivity. *Molecules* **2021,** 26 (8), DOI: 10.3390/molecules26082176.

34. Caravan, P.; Esteban-Gómez, D.; Rodríguez-Rodríguez, A.; Platas-Iglesias, C. Water exchange in lanthanide complexes for MRI applications. Lessons learned over the last 25 years. *Dalton Trans.* **2019,** 48 (30), 11161-11180 DOI: 10.1039/c9dt01948k.

35. Tóth, É.; Helm, L.; Merbach, A. In *The Chemistry of Contrast Agents in Medical Magnetic Resonance Imaging*; John Wiley & Sons, Ltd: 2013; pp 25-81.

36. Nicolle, G. M.; Tóth, É.; Eisenwiener, K.-P.; Mäcke, H. R.; Merbach, A. E. From monomers to micelles: investigation of the parameters influencing proton relaxivity. *JBIC Journal of Biological Inorganic Chemistry* **2002,** 7 (7), 757-769 DOI: 10.1007/s00775-002-0353-3.

37. Florès, O.; Pliquett, J.; Abad Galan, L.; Lescure, R.; Denat, F.; Maury, O.; Pallier, A.; Bellaye, P.-S.; Collin, B.; Même, S.; Bonnet, C. S.; Bodio, E.; Goze, C. Aza-BODIPY Platform: Toward an Efficient Water-Soluble Bimodal Imaging Probe for MRI and Near-Infrared Fluorescence. *Inorg. Chem.* **2020,** 59 (2), 1306-1314 DOI: 10.1021/acs.inorgchem.9b03017.

38. Jenni, S.; Bolze, F.; Bonnet, C. S.; Pallier, A.; Sour, A.; Tóth, É.; Ventura, B.; Heitz, V. Synthesis and In Vitro Studies of a Gd(DOTA)–Porphyrin Conjugate for Combined MRI and Photodynamic Treatment. *Inorg. Chem.* **2020,** 59 (19), 14389-14398 DOI: 10.1021/acs.inorgchem.0c02189.

39. Corsi, D. M.; Platas-Iglesias, C.; van Bekkum, H.; Peters, J. A. Determination of paramagnetic lanthanide(III) concentrations from bulk magnetic susceptibility shifts in NMR spectra. *Magn. Reson. Chem.* **2001,** 39 (11), 723-726 DOI: 10.1002/mrc.922.

40. Beeby, A.; Clarkson, I. M.; Dickins, R. S.; Faulkner, S.; Parker, D.; Royle, L.; de Sousa, A. S.; Williams, J. A. G.; Woods, M. Non-radiative deactivation of the excited states of europium, terbium and ytterbium complexes by proximate energy-matched OH, NH and CH oscillators: an improved luminescence method for establishing solution hydration states. *J. Chem. Soc., Perkin Trans. 2* **1999,** (3), 493-503 DOI: 10.1039/a808692c.

41. Yerly, F. *VISUALISEUR 2.3.5 and OPTIMISEUR 2.3.5*. Lausanne, Switzerland, 1999.

42. Raiford, D. S.; Fisk, C. L.; Becker, E. D. Calibration of methanol and ethylene glycol nuclear magnetic resonance thermometers. *Anal. Chem.* **1979,** 51 (12), 2050-2051 DOI: 10.1021/ac50048a040.

43. Meiboom, S.; Gill, D. Modified Spin - Echo Method for Measuring Nuclear Relaxation Times. *Rev. Sci. Instrum.* **1958,** 29 (8), 688-691 DOI: 10.1063/1.1716296.

44. Micskei, K.; Helm, L.; Brucher, E.; Merbach, A. E. Oxygen-17 NMR study of water exchange on gadolinium polyaminopolyacetates [Gd(DTPA)(H2O)]2- and [Gd(DOTA)(H2O)]- related to NMR imaging. *Inorg. Chem.* **1993,** 32 (18), 3844-3850 DOI: 10.1021/ic00070a013.

45. Hugi, A. D.; Helm, L.; Merbach, A. E. Water Exchange on Hexaaquavanadium(III): a Variable-Temperature and Variable-Pressure ^{17}O-NMR Study at 1.4 and 4.7 Tesla. *Helv. Chim. Acta* **1985,** 68 (2), 508-521 DOI: 10.1002/hlca.19850680224.

TOC Graphic:

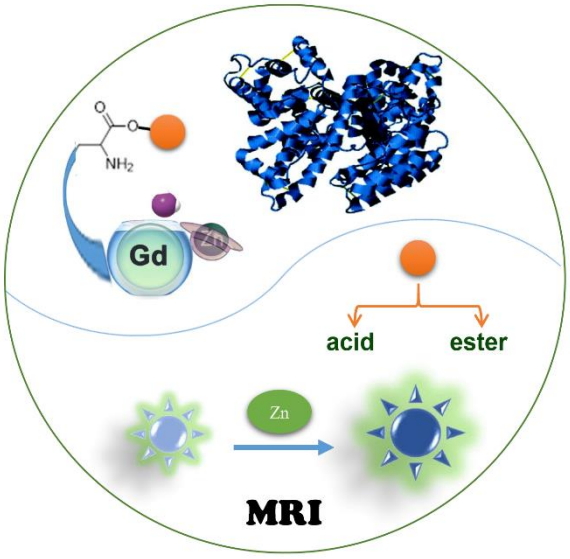

Synopsis

Two Gd-based and Zn-sensitive MRI probes were extensively studied by means of advanced NMR and isothermal titration calorimetry experiments. The conversion of a methyl ester to free carboxylic acid results in the modified coordination sphere of paramagnetic metal ions, which leads to different relaxivity responses, interaction with human serum albumin and distinct Zn-assisted aggregate formation. The obtained detailed insights are valuable for the future design and development of biocompatible responsive MRI probes.